Electronic band contraction induced low temperature methane activation on metal alloys

Victor Fung,[1]* Guoxiang Hu,[1] Bobby Sumpter[1]

[1]*Center for Nanophase Materials and Sciences, Oak Ridge National Laboratory, Oak Ridge, Tennessee 37831, United States*

**E-mail: fungv@ornl.gov Tel.: +1-951-384-5242*

Abstract

The catalytic conversion of methane under mild conditions is an appealing approach to selectively produce value-added products from natural gas. Catalysts which can chemisorb methane can potentially overcome challenges associated with its high stability and achieve facile activation. Although transition metals can activate C-H bonds, chemisorption and low-temperature conversion remains elusive on these surfaces. The broad electronic bands of metals can only weakly interact with the methane orbitals, in contrast to specific transition metal oxide and supported metal cluster surfaces which are now recognized to form methane σ-complexes. Here, we report methane chemisorption can, remarkably, occur on metal surfaces via electronic band contraction and localization from metal alloying. From a broad screening including single atom and intermetallic alloys in various substrates, we find early transition metals as promising metal solutes for methane chemisorption as well as low-temperature activation. These findings demonstrate a combinatorial diversity of possible candidates in earth abundant metal alloys with this attractive catalytic behavior.

1. Introduction

Methane is both a valuable energy source and a prime source of global warming. As a resource, vast untapped reserves of shale gas and methane hydrates remain on the planet which can provide fuel as well as be converted to value-added industrial products.[1, 2] As a greenhouse gas, methane's contribution is over 25 times larger than CO_2 by mass, and continues to rise in atmospheric concentration from anthropogenic sources.[3, 4] Catalytic materials which can capture and convert methane would serve dual purposes of removing unwanted greenhouse gas and converting fossil fuels to greener products. Methane catalytic conversion is often limited by the first C-H activation,[1, 5, 6] which is closely determined by the methane adsorption strength on the catalyst and the energy barrier for C-H cleavage. In particular, a strong methane chemisorption can promote facile C-H activation by the electronic weakening of the C-H bonds, and by shifting the C-H cleavage transition state energy below the molecular gas phase energy in a precursor-mediated mechanism.[7, 8, 9] The low-temperature activation of methane has recently received intense interest for its selective conversion under mild conditions.[9, 10, 11, 12]

Methane has been well-established to interact only weakly with metal surfaces in the form of physisorption on the order of approximately -0.1 to -0.2 eV.[7, 13, 14] Instead, reports of strong methane interaction in the literature have been limited thus far to either metal oxide surfaces or supported metal atoms and sub-nanometer clusters. Strong methane binding on oxide surfaces was observed on PdO,[15, 16] and RuO2,[8, 17] and IrO_2.[11, 18] Further theoretical studies have predicted similar phenomenon may manifest on β-PtO_2,[19] single-atom doped rutile oxides[20, 21] and doped ceria.[22] Supported metal adatoms and clusters such as Ni_1/CeO_2[10, 23] and Ni_4/TiC[9] have also been shown to exhibit similar low-temperature activation and conversion characteristics. A consistent picture of the electronic nature of the strong methane interaction in these systems can be linked to the localized, non-degenerate d-states in metal centers of oxides[19, 20, 21, 24] or molecule-like orbitals in metal clusters[25, 26, 27] which can hybridize with the methane C-H σ and σ* orbitals. Meanwhile, the broad, energetically degenerate d-band of metals interacts poorly with methane orbitals, while broad occupied s and p bands lead to a net repulsive interaction with the methane.[24, 28, 29] Only a few examples of weak chemisorption exist in the literature, with only Ir and Ru steps and kinks showing any appreciable interaction with methane.[30, 31, 32]

From a glance, it is evident metal surfaces are intrinsically unsuited for methane chemisorption and low-temperature activation compared to their oxide counterparts. Nonetheless, there exist several important reasons to revisit metal surfaces for this process. First, we hope to expand the list of known materials which can form methane complexes beyond the currently limited set of metal oxides and supported clusters from this study. There exists a high degree of structure and compositional sensitivity to specific oxide facets and sites shown in the literature[8, 15, 28, 33] such as for PdO(101) and rutile MO_2(110) or specific atomic sizes of supported clusters (ca. 5-10 atoms or less) which limits a high throughput search for these materials. In contrast, metals and their corresponding alloys represent a diverse set of possible catalysts hitherto unstudied for methane chemisorption and low-temperature conversion. Metal alloys containing inert metals such as Cu could additionally prevent overoxidation of products for improved selectivity as well as coking resistance.[34, 35] Using alloys with these metals would also circumvent the tendency of metal oxides and undercoordinated metal clusters to overbind to the products of methane activation, namely, the H and CH_3 moieties and their eventual overoxidation to CO_2. Finally, metal alloys containing earth abundant elements have shown promise as a viable inexpensive alternative to catalysts containing precious metals such as Pt, Pd, Ir, Rh.[36, 37, 38]

We propose a means to promote metal surfaces for methane chemisorption by engineering the contraction of the electronic bands of the metal surface sites from the formation of metal alloys, illustrated in Figure 1. Previously, density functional theory calculations and X-ray photoemission and adsorption studies have observed a substantial contraction of the d-band when a metal is alloyed into an inert host metal such as Cu, Ag and Au.[39, 40, 41] The weak hybridization of electron densities between the solute and solvent metals lead to the formation of an “atom-like” electronic structure in the solute metals, characterized by sharp, degenerate d bands similar to the free metal atom. We hypothesize a contraction of electronic bands could better mix with methane orbitals in much the same way as metal oxide centers and metal cluster edge sites, as well as reduce the repulsive interaction from the broad sp-band. We also observed more localized d_{z^2} states are conducive to stronger methane chemisorption in metal oxides in earlier studies.[21] We believe a corresponding localization of the d-band in metals will have a similar positive effect for methane complex formation.

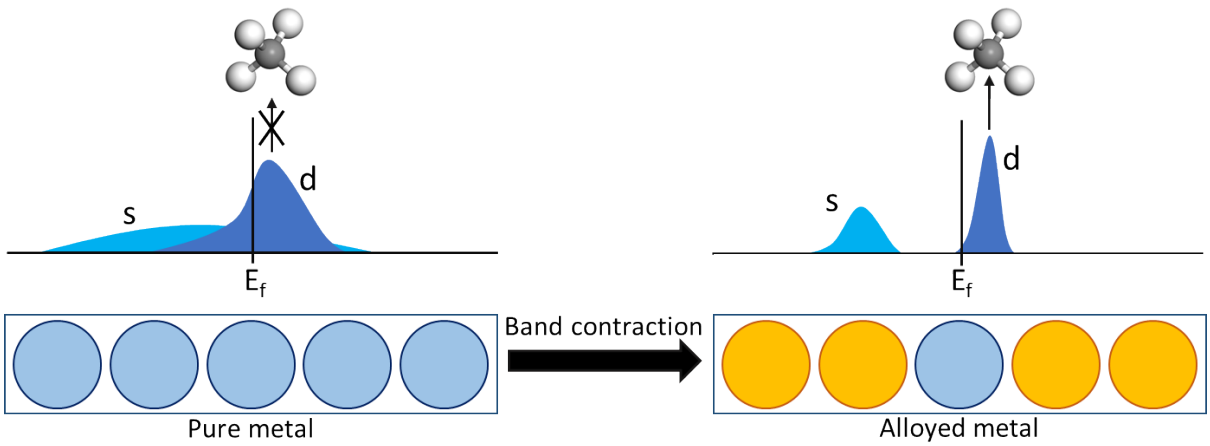

Figure 1: Scheme of alloying on metal electronic states and adsorbate interaction. The electronic structure change of the metal site before and after alloying is illustrated here. From the broad electronic bands of the pure metal (left), there is a subsequent narrowing and shift of the bands (right) when the metal is alloyed with an inert solvent metal. These narrowed bands, especially the d-band, would result in stronger methane interaction.

2. Results

2.1 Catalyst screening on single atom alloys

We begin the study by screening methane adsorption on the model system of a single atom site alloyed in an otherwise inert and weakly bonding substrate of copper. The coinage metal, copper, along with gold and silver, are well-established to weakly interact with the solute metal. Though single atom alloys in coinage metals have been well studied for catalysis,[34, 35, 39, 40, 42, 43, 44] to our knowledge no such study has been performed in the context of methane chemisorption and complex-mediated activation. We furthermore conduct the screening on four different Cu surface facets, (100), (111), (310) and (331) to model both flat terrace sites and step and kink sites. The (310) and (331) facets model steps intersecting the (100) and (111) terraces, respectively, which could serve as catalytically active sites as shown in the case of pure copper.[45, 46] To focus on chemisorption, we use the PBE functional with no van der Waals correction for the initial screening, such that an adsorption energy of zero approximately corresponds to a physisorption-only interaction. The results of the screening, organized in Figure 2, immediately reveals a wealth of possible methane chemisorbing alloys on all tested surface facets and a surprisingly large number of elements. It is evident methane chemisorption is indeed possible, even on flat (100) and (111) metal surfaces, in apparent validation of our approach.

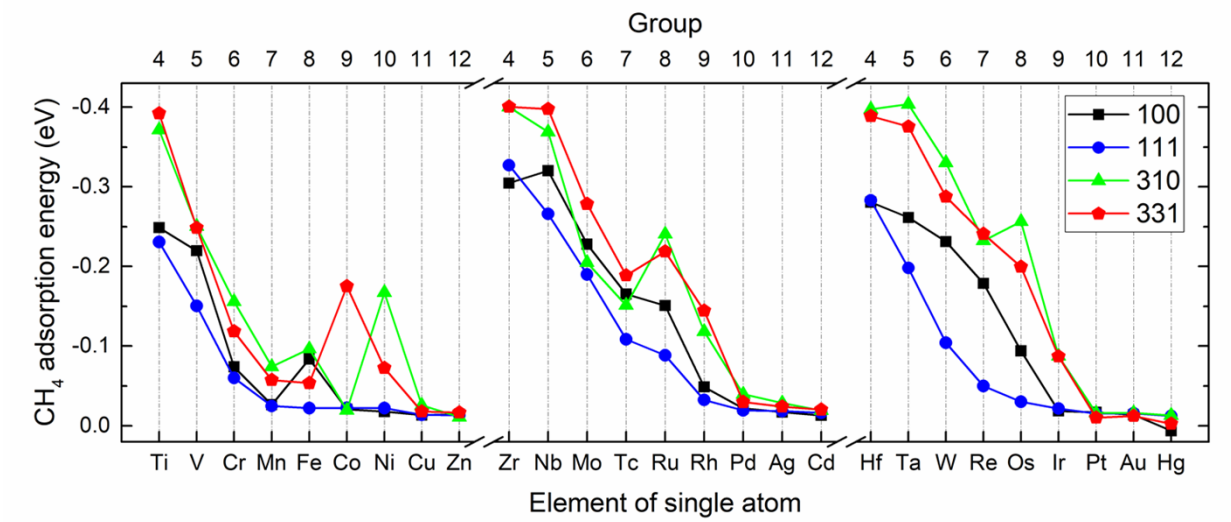

Figure 2: Methane chemisorption on M/Cu single atom copper alloys. Methane adsorption energies obtained with PBE, are plotted against the element of the solute single atom in copper. From left to right, the 3d, 4d and 5d transition metals were screened from groups 4 to 12. Four different surface facets of the copper substrate were tested, showing chemisorption can occur on all facets.

The methane chemisorption energies obtained on the single atom alloys are comparable to those on metal oxide surfaces and follow clear periodic trends. These energies can reach up to -0.40 eV on Zr/Cu(331), are larger than metals Ir(111) (-0.22 eV),[30] Ru(1010) (-0.10 eV),[32] metal oxides PdO(101) (-0.17 eV),[15] and RuO_2(110) (-0.18 ev),[18] and similar to IrO_2(110) at -0.37 to -0.41 eV[11, 18, 20] with the same level of theory. Of these, we find Ti, V, Zr, Nb, Mo, Ru, Hf, Ta, W, Re and Os with calculated adsorption energies larger than -0.2 eV using PBE. The strongest chemisorption appears to fall on the relatively overlooked group 4 metals Ti, Zr and Hf, and decreases nearly monotonically to group 12. Slight exceptions to the trend can be observed specifically for the high-index sites, with strong adsorption energies primarily in group 8 metals such as Ru and Os which is evocative of similar methane chemisorption on the pure Ru and Ir steps.[30, 32] In general, the higher index facets, (331) and (310), with exposed and undercoordinated metal sites exhibit stronger methane binding by roughly 0.1 to 0.2 eV. We expect electronic effects at play as well as the lower steric repulsion from the surrounding Cu atoms on the step sites behind the stronger adsorption. Surprisingly, the better-known single atom alloys such as Pt/Cu do not exhibit any chemisorption of methane of any kind. The clear periodic trends which favor the group 4 to group 6 metals and disfavor metals such as Pt and Pd strongly suggests d-electron count or d-band position and filling could have a primary role in determining methane chemisorption. We

will explore the mechanisms underlying these trends from electronic structure analyses in the subsequent sections.

2.2 Case study of chemisorption on Zr alloys

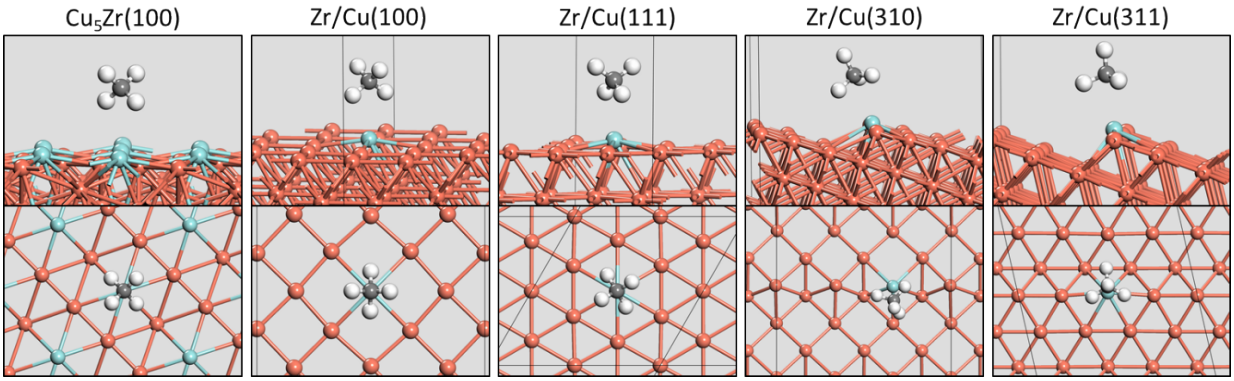

Figure 3: Methane chemisorption geometries on Zr/Cu. Geometries of the most stable adsorption geometries obtained with PBE are shown on the various intermetallic and single atom Zr/Cu alloys (C=grey, H=white, Zr=light blue, Cu=orange). Energies and bond lengths are compiled in table 1.

We investigate the role of alloying here in the case study of Zr, which was revealed to exhibit one of the strongest methane adsorption energies when alloyed in Cu. The adsorption energies between the single atom alloys in different Cu facets Zr/Cu(100), Zr/Cu(111), Zr/Cu(310), and Zr/Cu(331) are compared with pure Cu(100) and fcc Zr(100) as well as the intermetallic alloy phase $Cu_5Zr(100)$[47, 48] in table 1. With PBE, no apparent chemisorption was found on either Cu(100) or Zr(100) having energies close to zero, though the C-M distance on Zr(100) is lower by ~0.5 Å with a correspondingly lower adsorption energy by 0.04 eV. These minute differences could be a possible hint towards the enhanced chemisorption strength of Zr in its alloyed form, but nonetheless it is clear neither component metal has any significant interaction with methane. Moving to the intermetallic alloy $Cu_5Zr(100)$, methane was found to chemisorb (as well as on other surface facets shown in the supporting information) with an significant adsorption energy of -0.22 eV and a further decreased C-M distance of 2.834 Å. This finding is highly intriguing as it suggests the single atom criterion is not as strict as previously thought for the case of methane chemisorption, which is promising for the practical application of these catalysts. Finally, the Zr/Cu single atom alloys are found to have the strongest adsorption ranging from -0.3-0.4 eV. There does appear to be a slight benefit to extreme dilution of Zr, though the intermetallic alloys could still serve as active catalysts.

On $Cu_5Zr(100)$, Zr/Cu(100) and Zr/Cu(111), we find a stable methane adsorption geometry in the form of η-H,H in the nomenclature for transition metal complexes,[49] whereas on the Zr/Cu(310) and Zr/Cu(331) cases, a η-H,H,H geometry was slightly more favorable. A comparison between η-H,H and η-H,H,H adsorption energies for M/Cu(331) can be found in the supporting information, where we find energetic differences between the two adsorption geometries to be around 0.1 eV. Thus, on metal alloys surfaces, one would expect both adsorption geometries would be detectable due to similar energetics. Here, the C-M distance is a strong indicator of methane chemisorption, as the Zr/Cu alloy cases have distances well within the combined van der Waals radius of Zr and C (4.29 Å), and ranges from 2.8-2.5 Å. A lengthening of the C-H bond can moreover be observed with lengths of ~1.11 Å.

Table 1: Comparison of methane chemisorption on Zr/Cu alloys

Surface	Cu(100)	Zr(100)	$Cu_5Zr(100)$	Zr/Cu(100)	Zr/Cu(111)	Zr/Cu(310)	Zr/Cu(331)
PBE E_{ads} (eV)	-0.01	-0.05	-0.22	-0.30	-0.33	-0.40	-0.40
C-M distance (Å)	3.563	3.060	2.822	2.765	2.735	2.549	2.554
C-H distance (Å)	1.098	1.108	1.110	1.112	1.114	1.116	1.113
PBE+D3 E_{ads} (eV)	-0.25	-0.26	-0.43	-0.56	-0.59	-0.62	-0.62
C-M distance (Å)	3.125	3.016	2.834	2.720	2.689	2.514	2.513
C-H distance (Å)	1.101	1.109	1.110	1.114	1.116	1.118	1.115
SCAN+rVV10 E_{ads} (eV)	-0.26	-0.36	-0.71	-0.73	-0.70	-0.86	-0.88
C-M distance (Å)	3.600	3.110	2.834	2.718	2.798	2.513	2.528
C-H distance (Å)	1.098	1.120	1.082	1.121	1.104	1.121	1.118

We further extend our calculations on these systems to include van der Waals corrections, using the D3 damped atomic potential[50] and the nonlocal correlation functional rVV10 paired with the accurate meta-generalized gradient approximation functional SCAN.[51, 52] SCAN+rVV10 was chosen due to excellent agreement for energies and geometries for the adsorption of hydrocarbons such as benzene on coinage metals, outperforming most other functionals.[52] Previous studies on methane chemisorbed complexes have emphasized the need for dispersion corrections to accurate predict experimental adsorption energies, where the dispersion accounts for approximately 30-60 percent of the total adsorption energy.[15, 33] On metal surfaces we similarly find the D3 correction to add roughly 0.2 eV to the total adsorption energy across the board, which brings the non-chemisorbing surfaces to around -0.2 to -0.3 eV and the chemisorbing ones up to -0.62 eV. Here,

we expect the van der Waals correction to preserve the relative energy trends observed in Figure 2. Interestingly, the SCAN+rVV10 functional increases binding energies of the Zr-containing surfaces even further than PBE-D3, especially in bringing the $Cu_5Zr(100)$ energy to a level comparable to the single atom cases. The strongest adsorption energies using SCAN+rVV10 reach up to -0.88 eV for Zr/Cu(331), though we would expect overbinding could occur for this method. Further theoretical validation and eventual experimental data are needed to pinpoint the exact methane adsorption energies on these alloys, though the PBE-only and SCAN+rVV10 energies can conceivably serve as plausible upper and lower energetic bounds.

2.3 Low-temperature activation of methane

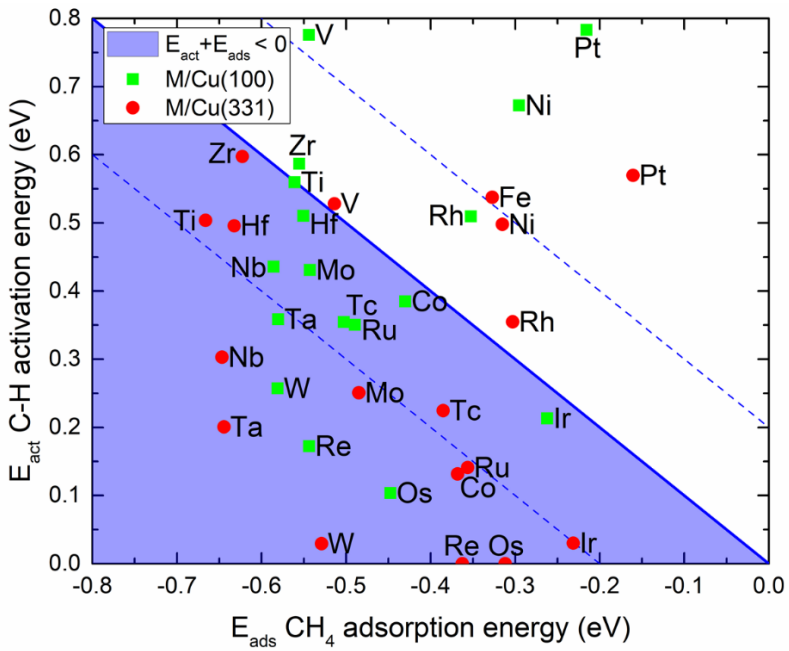

Figure 4: Methane adsorption and activation energies. Methane adsorption and activation energies over M/Cu(100) and M/Cu(331) surfaces calculated using PBE+D3 are plotted. The region in blue denotes where the desorption energy of methane is higher than the its activation barrier, predicting where facile methane activation is likely to occur. The shaded lines show the approximate range of error within 0.2 eV arising from the functional choice. Methane activation energies up to 0.8 eV are plotted, with the full list of surfaces shown in the supplementary information.

Given the methane chemisorption energies comparable to those on metal oxides, similar low-temperature activation is expected on metal alloys. We screen the methane activation barriers over the low-index M/Cu(100) and high-index M/Cu(331) surfaces using PBE+D3, shown in Figure 4. The blue region in the figure indicates where desorption of methane to the gas phase lies higher in

energy than its activation. To date, $IrO_2(110)$ is the only surface which has been found through experimental and theoretical studies to exhibit this behavior, with methane activation occurring as low as 150K.[11, 18] In the 48 single atom alloys we screened, we find over 20 with this predicted behavior, with many more to be expected from additional bimetallic combinations. Promising single atom alloys include Ta, W, Re, and Os in Cu(100) and Nb, Ta, and W, Os, and Ru in Cu(331), and are primarily found containing early to mid transition metal elements. In comparison, pure Cu(110) and Cu(331) are poor surfaces for methane activation with barriers of 1.39 and 1.20 eV, respectively, and the single atom alloys of traditional methane conversion catalysts such as Ni and Pt still fall well beyond this region. While the higher index surface performed better overall with stronger chemisorption and lower activation barriers, both low and high index surfaces contained alloys where facile methane activation is possible.

Another important observation is that the obtained activation energies of the alloys where chemisorption is present (early and mid transition metals) are significantly lower compared to their pure metal counterparts. For example, the barrier is reduced from 0.74 eV on pure Zr(100) to 0.43 eV on Zr/Cu(100), as seen in supplementary figure 1. In contrast, for the late transition metals with no chemisorption such as Pt, the single atom alloy form has a *higher* activation barrier than the pure Pt metal, as it was hypothesized the activity had been quenched by the relatively inert Cu.[35] These results strongly suggest methane chemisorption over the early and mid transition metals reduces the C-H activation barriers, which is consistent with the observation of a lengthened C-H bond in the chemisorbed methane.

We further obtained free-energy profiles for methane first C-H activation using PBE+D3 under a range of temperatures, shown in Figure 5. We chose Re/Cu(100) and Ta/Cu(331) as promising candidates from both low and high index surfaces with a combination of both strong chemisorption and low activation barriers. While Zr/Cu exhibits the strongest chemisorption, it also has a comparatively higher activation barrier. The energy profiles from these two surfaces show facile activation up to 300K similar to oxides such as $IrO_2(110)$. For both tested facets, activation occurs via a chemisorbed initial state, followed by C-H cleavage by a M-Cu pair (M being the single atom dopant). The obtained transition state contains a hydrogen coordinated to both M and Cu. Following C-H cleavage, the methyl remains bonded to M, while the H binds to a nearby hollow

site. The dissociation is exothermic on both surfaces. A complete list of the adsorption, activation and dissociation energies can be found in the supplementary information.

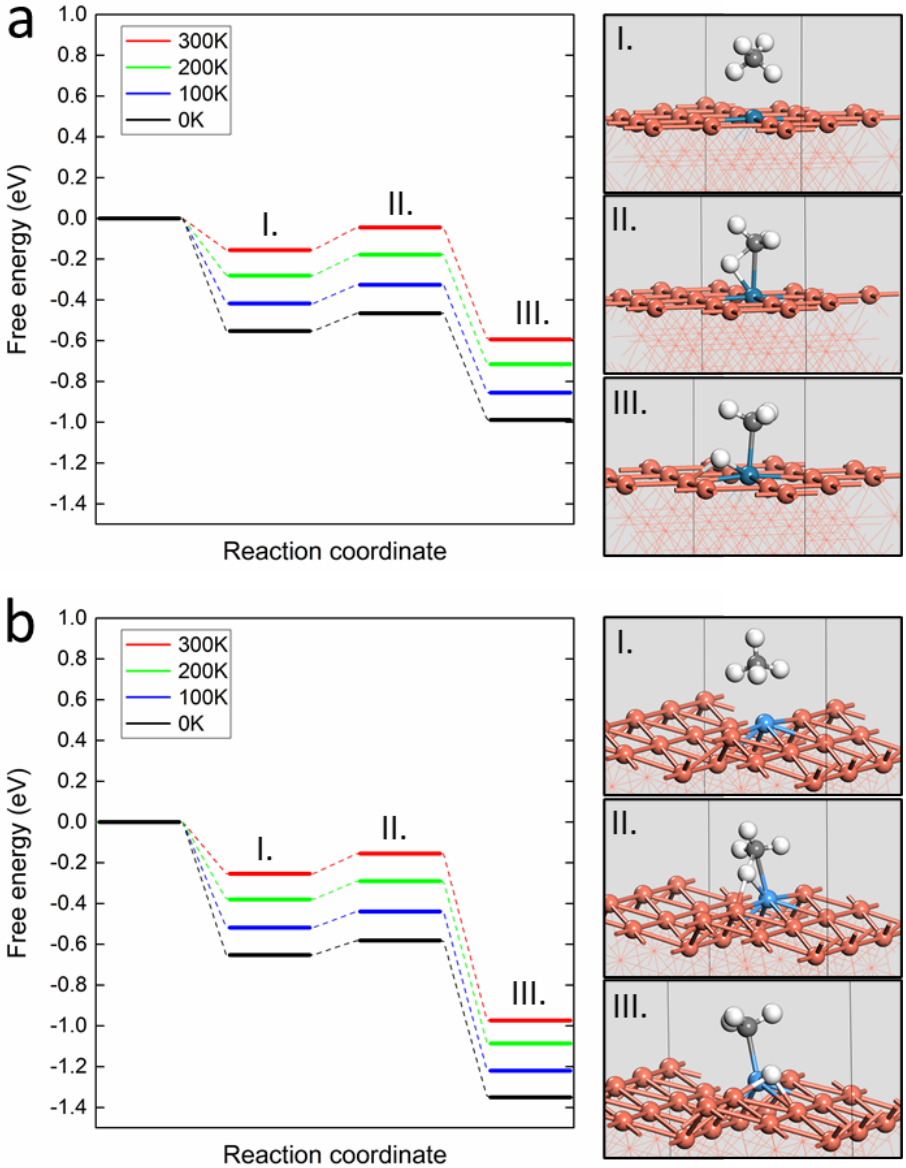

Figure 5: Energy profile of methane activation on single atom alloys. The free energies of methane dissociation on **(a)** Re/Cu(100) and **(b)** Ta/Cu(331) are shown at various temperatures from 0-300K calculated using PBE+D3 including zero-point and vibrational contributions to entropy. The geometries of the initial chemisorbed state I., the transition state II., and the final state III. are shown to the right.

2.4 Electronic properties of the methane surface complex

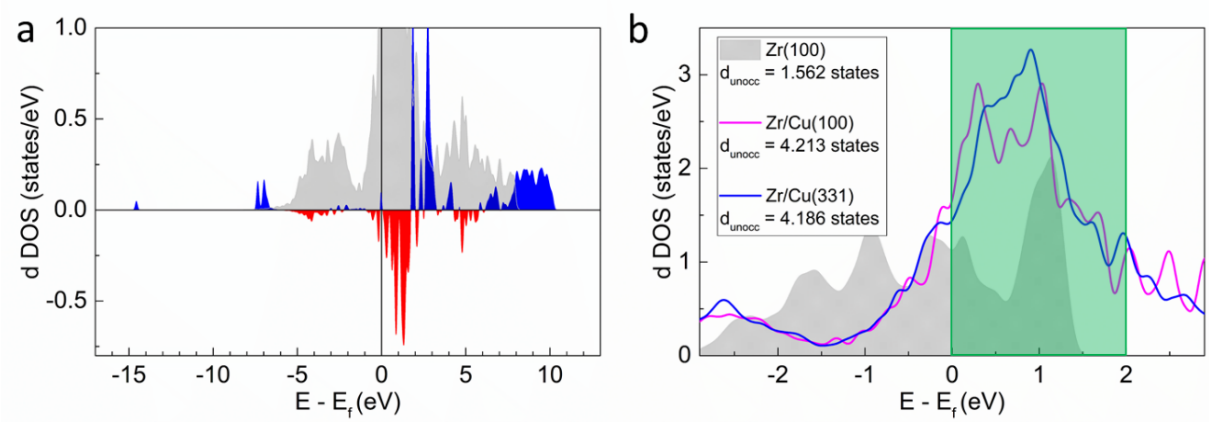

Figure 6: Electronic structure of the Zr/Cu alloy and methane chemisorbed complex. (a) Density of states difference plot of the Zr atom in Zr/Cu(100) before and after methane chemisorption overlaid over the initial density of states (in grey). Decrease in states are shown in red and increase is shown in blue. **(b)** The projected density of states of Zr in Zr/Cu(100) and Zr/Cu(331) single atom alloys are compared with the Zr surface atom in pure Zr(100) shown in grey. The green region highlights states near the Fermi level from 0 to 2 eV as the integration range for d_{unocc}, with the values shown in the legend.

The results thus far show clear proof of methane chemisorption and activation on single atom alloys; we now seek to demonstrate a causal link between the electronic structure of the substrate and chemisorption. We begin by investigating the electronic structure of the chemisorbed methane complex on Zr/Cu(100). The density of states difference plot for the same methane complex is shown in Figure 6a, which shows a clear depletion of empty d states (shown in red) in the region above the Fermi level from 0 to 2 eV, which is indicative of a dative interaction involving electron donation from methane C-H bonds into the empty metal states. A possible back-bonding interaction from filled d-states can also be observed from the slight depletion in the d-band from -5 to 0 eV below the Fermi level, though further analysis is warranted to identify this interaction. The observed hybridization of d-states above the Fermi level is characteristic of methane complexes in other surfaces such as metal oxides.[18, 19, 20, 21]

A look at the density of states plot of the Zr/Cu single atom alloys in comparison with pure Zr indeed shows signs of electronic band contraction, as shown in Figure 5b. Overall, the d states are clearly localized in the region centered around 0.5 eV relative to the Fermi level compared to pure Zr to form a distinct peak rather than a broad band. The observed d-band contraction falls short of the "free-atom-like" description for single atom alloys such as Ag/Cu,[39, 40] though the fact that

methane chemisorption can still occur on Zr/Cu over the pure Zr metal suggests even a lesser degree of contraction can have a substantial improvement. We calculate the number of empty or unoccupied d-states in the relevant 0 to 2 eV region (d_{unocc}) in Figure 6b highlighted in green and find approximately 2.5-3 times the number of empty states available for donation by methane in Zr/Cu over the pure Zr, which further corroborates with the observed chemisorption.

From the electronic structure pure in Figure 6, it is clear the methane chemisorption strength is closely linked to the number of available empty states for electron donation by methane. Here, we try to correlate these electronic descriptors with the adsorption energies. First of these is the d-band center, which has already been extensively used to predict adsorption properties for transition metals, plotted in Figure 7a.[53] Here, we find a lower d-band center (d_{center}) to approximately correlate to a weaker methane adsorption, with an R^2 of 0.66 in the energy region where methane chemisorption is non-zero. Next, we plot the number of empty or unoccupied d-states (d_{unocc}) in Figure 7b. When considering the 4d and 5d transition metals, the correlation with adsorption energy works remarkably well, with an R^2 of 0.94, though the energies for the 3d metals are consistently underestimated. One such reason for lower-than-expected energies is the greater contraction of the 3d orbitals which leads to a weaker degree of hybridization.[20] From these descriptors qualitative predictions can be made, though it is clear other factors can play a role in the chemisorption energy of methane. Consequently, linear correlations containing individual descriptors become insufficient to capture all the interactions of the methane complex.

We turn to statistical learning to sample the feature space containing all the possible electronic parameters involved in determining methane chemisorption, which can aid in descriptor identification and the development of quantitative predictive models.[54, 55] In our feature space we included solely electronic properties, which are the number of empty s, p and d states from 0 to 2 eV, number of filled s, p and d states from -2 to 0 eV, the s, p and d centers spanning the full energy range, and additionally the s, p and d orbital radii.[56] We used a compressed sensing method, SISSO (sure independence screening and sparsifying operator), to identify the best linear combination of candidate features from the space $\Phi_{1\text{-}3}$.[57] Here, Φ_n is constructed from Φ_0 containing the twelve aforementioned primary features. A search over this space reveals a 1D Φ_2 descriptor with lowest RMSE which provides a fit with R^2=0.94 (Figure 7c):

$$Eads = -0.436 * 10^{-1} * \frac{r_p * d_{unocc} * p_{unocc}^{0.5}}{\frac{p_{occ} + s_{occ}}{\log(r_p)}} - 0.666 * 10^{-2}$$

We find the adsorption energy is proportional to the number of empty d and p states (d_{unocc}, p_{unocc}) which determine the degree of electron transfer from the methane C-H bond to the metal site, and inversely proportion to the number of filled s and p states (s_{occ}, p_{occ}), which can modulate the repulsive interaction between the methane and the surface. Finally, the orbital radii (r_p) is present in the descriptor due to its role in determining degree of overlap with methane orbitals. Using compressed sending, we are therefore able to obtain a simple analytical expression describing methane adsorption energy in close agreement with the observed physical picture of methane chemisorption, which also performs significantly better than conventional descriptors such as the d-band center (Figure 7a).

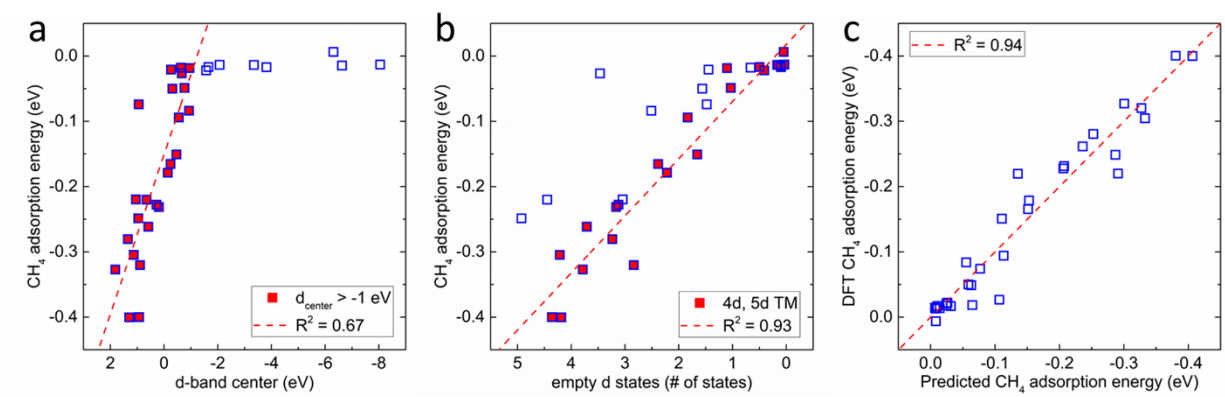

Figure 7: Descriptors for methane adsorption. (a) Correlations between individual descriptors, d-band center (left) and **(b)** # of empty d states (right), with methane adsorption energy using PBE. Linear best fits (red dashed lines) are plotted for the selected points in red, which correspond to points with a d_{center} above -1 eV, and the 4d and 5d transition metals. (**c)** Correlation between the predicted adsorption energies from SISSO-derived expression and the DFT energies with linear best fit in red dashed lines applied to all points.

Overall, we demonstrate the availability of electron acceptor states to have a primary contribution to methane chemisorption, followed by the repulsion from the sp bands, and finally the orbital radii which further determine the degree of orbital overlap. It is clear the first two contributions listed above are aided by the alloying effect in metals and corresponding electronic band contraction. In particular, the contracted d band observed in Figure 4 can allow for more

states to exist within the relevant energy window (ca. 0 to 2 eV) for methane bonding. The amount of electron acceptor states is also further influenced by the identity of the metal solute, whose intrinsic d-band position determines where the peak of d-states will fall once alloyed. This explains the favorability of early transition metal solutes (Ti, Zr, Hf) towards methane chemisorption due to their high d-band centers in their pure forms, whereas the later transition metals with lower d-band centers (Ni, Pd, Pt) have d-states which are almost completely occupied regardless of band contraction. The identity of the metal furthermore determines the orbital radii, which is why chemisorption on flat (100) and (111) surfaces is favored for the 4d and 5d metals with wider radii than the 3d, though these differences vanish on the high-index surfaces due to the solute atom becoming more exposed on the surface.

2.5 Stability and expansion to other metal alloys

Table 2: Comparison of methane chemisorption on Zr alloyed in different metal substrates

Surface	Zr/Co(100)	Zr/Ni(100)	Zr/Ag(100)	Zr/Au(100)
PBE E_{ads} (eV)	-0.24	-0.25	-0.25	-0.29
C-M distance (Å)	2.829	2.822	2.784	2.770
C-H distance (Å)	1.110	1.110	1.114	1.113

Finally, the exceptional performance of Zr and other metals alloyed in Cu raises the question of whether Cu has an exclusive role in the activity of the solute metal. An additional sampling of four additional solvent metals Co, Ni, Ag, and Au is organized in Table 2. Ag and Au, being in the same coinage group, show similar energies with Cu as anticipated. Unexpectedly, we find even the non-coinage metals, Co and Ni, could serve as effective substrates, though the interactions are slightly weaker by ca. 0.05 eV with marginally longer corresponding C-M distances. As revealed earlier in Figure 4, true free-atom-like states are not a necessary condition for chemisorption, though it may certainly aid in a stronger interaction. Instead, a general contraction of the bands and a sufficient amount of empty states in the region above the Fermi level appears to be adequate to allow for methane complex formation. To this end, the degree of dilution and the elemental identity of the solute metal appear to be the primary determinants in chemisorption strength.

This observation is highly encouraging for the materials design of active catalysts as it suggests an extensive range of possible alloy combinations and stoichiometry where methane chemisorption and facile activation can occur. Within just the bimetallic regime, there exist several thousand

combinations of the solute metals identified in this work (such as Ti, V, Zr, Nb, Mo, Ru, Hf, Ra, W, Re and Os) with the various metal solvents beyond Cu, and in concentrations ranging from the single-atom limit to stochiometric intermetallic compounds. Further modifications can also be applied onto this alloying framework, such as strain and coordination-based modification to induce further band narrowing and upshift.[58, 59] These adsorption properties can be calculated with an appropriate DFT functional or quickly screened via the electronic descriptors identified in this work.

Significant advances in metal alloy synthesis have made the predicted materials experimentally accessible,[60, 61] such as through wet chemistry methods,[62, 63] physical vapor deposition,[64] or more recent 'thermal shock' techniques.[65, 66] Another concern is whether the active solute metal will remain on the surface or become hidden in the subsurface. Under reaction conditions, the presence of reactants and intermediates is known to draw the more reactive metal to the surface,[67, 68] which we find to be similarly true for many of the studied single atom alloys in this work. On Re/Cu(100) and Ta/Cu(331), we find the segregation energy of the dopant to be 0.27 eV and 0.36 eV, respectively, in the presence of methyl and hydrogen species on the surface (supplementary figure 3). Here, a positive energy denotes a thermodynamically unfavorable transition from the surface to the subsurface, aided by the fact that Cu is comparatively more inert and binds much more weakly to methyl and hydrogen than the dopants.

3. Conclusion

We have investigated whether metal alloys can act as viable surfaces for the chemisorption and low-temperature activation of methane, via an exhaustive screening of single atom alloys in Cu and several other substrates. We hypothesized the shift and contraction of the electronic states of the metal site in the alloy would allow for chemisorption to occur which would otherwise be impossible in the pure metal. From our screening, we have revealed unprecedented cases of strong chemisorption and facile activation over metal surfaces such as Re/Cu(100) and Ta/Cu(331). Clear energetic trends were also observed which favor the early to mid-transition metals. Electronic structure and statistical learning analyses reveal electron donation from methane to empty metal d states as the primary contributor to the formation of the chemisorbed complex, which can be predicted from d-band center and d-occupancy based descriptors. The origin of strong chemisorption on alloys can be attributed to both the high intrinsic d-band center of the solute

metals and the contraction of the solute electronic bands from alloying. Metal alloys which exhibit strong chemisorption furthermore show reduced C-H activation barriers, which can lead to facile methane activation under 300K. Therefore, metal alloys show significant promise as a class of inexpensive low-temperature methane conversion catalysts which encompass a broad range of possible stoichiometries, surface geometries, and elemental compositions of the solute and solvent metals.

Acknowledgements

This work was supported by the Center for Understanding and Control of Acid Gas-Induced Evolution of Materials for Energy (UNCAGE-ME), an Energy Frontier Research Center funded by U.S. Department of Energy (US DoE), Office of Science, Basic Energy Sciences (BES), under Award DE-SC0012577. Work was performed at the Center for Nanophase Materials Sciences, a US Department of Energy Office of Science User Facility. VF was also supported by a Eugene P. Wigner Fellowship at Oak Ridge National Laboratory. This research used resources of the National Energy Research Scientific Computing Center, supported by the Office of Science of the U.S. Department of Energy under Contract No. DE-AC02-05CH11231.

Author Contributions

VF conceived the project and conducted the calculations. All authors contributed to the writing of the manuscript.

Competing Interests

The authors declare no competing interests.

Additional Information

Supplementary information is available.

References

1. Horn R, Schlögl R. Methane Activation by Heterogeneous Catalysis. *Catal Lett* **145**, 23-39 (2015).
2. Schwach P, Pan X, Bao X. Direct Conversion of Methane to Value-Added Chemicals over Heterogeneous Catalysts: Challenges and Prospects. *Chem Rev* **117**, 8497-8520 (2017).
3. Bousquet P*, et al.* Contribution of anthropogenic and natural sources to atmospheric methane variability. *Nature* **443**, 439-443 (2006).
4. Solomon S, Qin D, Manning M, Averyt K, Marquis M. *Climate change 2007-the physical science basis: Working group I contribution to the fourth assessment report of the IPCC*. Cambridge university press (2007).
5. Lunsford JH. The Catalytic Oxidative Coupling of Methane. *Angew Chem Int Ed* **34**, 970-980 (1995).
6. Latimer AA*, et al.* Understanding Trends in CH Bond Activation in Heterogeneous Catalysis. *Nat Mater* **16**, 225-229 (2017).
7. Weaver JF, Carlsson AF, Madix RJ. The adsorption and reaction of low molecular weight alkanes on metallic single crystal surfaces. *Surf Sci Rep* **50**, 107-199 (2003).

8. Weaver JF, Hakanoglu C, Antony A, Asthagiri A. Alkane activation on crystalline metal oxide surfaces. *Chem Soc Rev* **43**, 7536-7547 (2014).
9. Prats H*, et al.* Room Temperature Methane Capture and Activation by Ni Clusters Supported on TiC(001): Effects of Metal–Carbide Interactions on the Cleavage of the C–H Bond. *J Am Chem Soc* **141**, 5303-5313 (2019).
10. Lustemberg PG*, et al.* Room-Temperature Activation of Methane and Dry Re-Forming With CO_2 On Ni-CeO_2 (111) Surfaces: Effect of Ce^{3+} Sites and Metal–Support Interactions on C–H Bond Cleavage. *ACS Catal* **6**, 8184-8191 (2016).
11. Liang Z, Li T, Kim M, Asthagiri A, Weaver JF. Low-Temperature Activation of Methane on the IrO_2 (110) Surface. *Science* **356**, 299-303 (2017).
12. Cui X*, et al.* Room-Temperature Methane Conversion by Graphene-Confined Single Iron Atoms. *Chem* **4**, 1902-1910 (2018).
13. Wellendorff J*, et al.* A benchmark database for adsorption bond energies to transition metal surfaces and comparison to selected DFT functionals. *Surf Sci* **640**, 36-44 (2015).
14. Tait SL, Dohnálek Z, Campbell CT, Kay BD. n-alkanes on Pt(111) and on C(0001)/Pt(111): Chain length dependence of kinetic desorption parameters. *J Chem Phys* **125**, 234308 (2006).
15. Weaver JF, Hakanoglu C, Hawkins JM, Asthagiri A. Molecular Adsorption of Small Alkanes on a PdO(101) Thin Film: Evidence of Sigma-Complex Formation. *J Chem Phys* **132**, 024709 (2010).
16. Antony A, Asthagiri A, Weaver JF. Pathways and kinetics of methane and ethane C–H bond cleavage on PdO(101). *J Chem Phys* **139**, 104702 (2013).
17. Li T, Kim M, Rai R, Liang Z, Asthagiri A, Weaver JF. Adsorption of alkanes on stoichiometric and oxygen-rich RuO_2(110). *Phys Chem Chem Phys* **18**, 22647-22660 (2016).
18. Wang C-C, Siao SS, Jiang J-C. C–H Bond Activation of Methane via σ–d Interaction on the IrO_2 (110) Surface: Density Functional Theory Study. *J Phys Chem C* **116**, 6367-6370 (2012).
19. Tsuji Y, Yoshizawa K. Adsorption and Activation of Methane on the (110) Surface of Rutile-type Metal Dioxides. *J Phys Chem C* **122**, 15359-15381 (2018).
20. Fung V, Tao F, Jiang D-e. Low-Temperature Activation of Methane on Doped Single Atoms: Descriptor and Prediction. *Phys Chem Chem Phys* **20**, 22909-22914 (2018).
21. Fung V, Hu G, Tao FF, Jiang DE. Methane Chemisorption on Oxide-Supported Pt Single Atom. *ChemPhysChem* **20**, 2217-2220 (2019).
22. Su Y-Q, Liu J-X, Filot IAW, Zhang L, Hensen EJM. Highly Active and Stable CH4 Oxidation by Substitution of Ce4+ by Two Pd2+ Ions in CeO2(111). *ACS Catal* **8**, 6552-6559 (2018).
23. Liu Z*, et al.* In Situ Investigation of Methane Dry Reforming on Metal/Ceria(111) Surfaces: Metal–Support Interactions and C−H Bond Activation at Low Temperature. *Angew Chem Int Ed* **56**, 13041-13046 (2017).
24. Saillard JY, Hoffmann R. Carbon-Hydrogen and Hydrogen-Hydrogen Activation in Transition Metal Complexes and on Surfaces. *J Am Chem Soc* **106**, 2006-2026 (1984).
25. Schwarz H, Shaik S, Li J. Electronic Effects on Room-Temperature, Gas-Phase C–H Bond Activations by Cluster Oxides and Metal Carbides: The Methane Challenge. *J Am Chem Soc* **139**, 17201-17212 (2017).
26. Zhou S, Li J, Schlangen M, Schwarz H. The Origin of the Efficient, Thermal Chemisorption of Methane by the Heteronuclear Metal-Oxide Cluster [Al2TaO5]+. *Angew Chem Int Ed* **55**, 14867-14871 (2016).
27. Harding DJ, Kerpal C, Meijer G, Fielicke A. Activated Methane on Small Cationic Platinum Clusters. *Angew Chem Int Ed* **51**, 817-819 (2012).
28. Hellman A*, et al.* The Active Phase of Palladium during Methane Oxidation. *J Phys Chem Lett* **3**, 678-682 (2012).
29. van Santen RA, Tranca I, Hensen EJ. Theory of Surface Chemistry and Reactivity of Reducible Oxides. *Catal Today* **244**, 63-84 (2015).
30. Henkelman G, Jónsson H. Theoretical Calculations of Dissociative Adsorption of CH4 on an Ir(111) Surface. *Phys Rev Lett* **86**, 664-667 (2001).

31. Arevalo RL, Aspera SM, Escaño MCS, Nakanishi H, Kasai H. First principles study of methane decomposition on B5 step-edge type site of Ru surface. *J Phys: Condens Matter* **29**, 184001 (2017).
32. Shetty S, Jansen APJ, van Santen RA. Methane Formation on Corrugated Ru Surfaces. *J Phys Chem C* **114**, 22630-22635 (2010).
33. Antony A, Hakanoglu C, Asthagiri A, Weaver JF. Dispersion-corrected density functional theory calculations of the molecular binding of n-alkanes on Pd(111) and PdO(101). *J Chem Phys* **136**, 054702 (2012).
34. Giannakakis G, Flytzani-Stephanopoulos M, Sykes ECH. Single-Atom Alloys as a Reductionist Approach to the Rational Design of Heterogeneous Catalysts. *Acc Chem Res* **52**, 237-247 (2019).
35. Marcinkowski MD*, et al.* Pt/Cu single-atom alloys as coke-resistant catalysts for efficient C–H activation. *Nat Chem* **10**, 325 (2018).
36. He Y, Song Y, Cullen DA, Laursen S. Selective and Stable Non-Noble-Metal Intermetallic Compound Catalyst for the Direct Dehydrogenation of Propane to Propylene. *J Am Chem Soc* **140**, 14010-14014 (2018).
37. Armbrüster M*, et al.* Al13Fe4 as a low-cost alternative for palladium in heterogeneous hydrogenation. *Nat Mater* **11**, 690 (2012).
38. Furukawa S, Komatsu T. Intermetallic Compounds: Promising Inorganic Materials for Well-Structured and Electronically Modified Reaction Environments for Efficient Catalysis. *ACS Catal* **7**, 735-765 (2017).
39. Greiner MT*, et al.* Free-atom-like d states in single-atom alloy catalysts. *Nat Chem* **10**, 1008-1015 (2018).
40. Thirumalai H, Kitchin JR. Investigating the Reactivity of Single Atom Alloys Using Density Functional Theory. *Top Catal* **61**, 462-474 (2018).
41. Inderwildi OR, Jenkins SJ, King DA. When adding an unreactive metal enhances catalytic activity: NOx decomposition over silver–rhodium bimetallic surfaces. *Surf Sci* **601**, L103-L108 (2007).
42. Li H, Chai W, Henkelman G. Selectivity for ethanol partial oxidation: the unique chemistry of single-atom alloy catalysts on Au, Ag, and Cu(111). *J Mater Chem A*, (2019).
43. Duchesne PN*, et al.* Golden single-atomic-site platinum electrocatalysts. *Nat Mater* **17**, 1033-1039 (2018).
44. Zhu X*, et al.* Optimising surface d charge of AuPd nanoalloy catalysts for enhanced catalytic activity. *Nat Commun* **10**, 1428 (2019).
45. Hagman B*, et al.* Steps Control the Dissociation of CO2 on Cu(100). *J Am Chem Soc* **140**, 12974-12979 (2018).
46. Fu SS, Somorjai GA. Interactions of O_2, CO, CO_2, and D_2 with the stepped Cu(311) crystal face: Comparison to Cu(110). *Surf Sci* **262**, 68-76 (1992).
47. Zhou SH, Napolitano RE. Phase stability for the Cu–Zr system: First-principles, experiments and solution-based modeling. *Acta Mater* **58**, 2186-2196 (2010).
48. Yi G*, et al.* Mechanical, electronic and thermal properties of Cu5Zr and Cu5Hf by first-principles calculations. *J Alloys Compd* **640**, 455-461 (2015).
49. Hall C, Perutz RN. Transition Metal Alkane Complexes. *Chem Rev* **96**, 3125-3146 (1996).
50. Grimme S, Antony J, Ehrlich S, Krieg H. A Consistent and Accurate ab Initio Parametrization of Density Functional Dispersion Correction (DFT-D) for the 94 Elements H-Pu. *J Chem Phys* **132**, 154104 (2010).
51. Sun J, Ruzsinszky A, Perdew JP. Strongly Constrained and Appropriately Normed Semilocal Density Functional. *Phys Rev Lett* **115**, 036402 (2015).
52. Peng H, Yang Z-H, Perdew JP, Sun J. Versatile van der Waals Density Functional Based on a Meta-Generalized Gradient Approximation. *Physical Review X* **6**, 041005 (2016).
53. Nørskov JK, Bligaard T, Rossmeisl J, Christensen CH. Towards the Computational Design of Solid Catalysts. *Nat Chem* **1**, 37-46 (2009).

54. O'Connor NJ, Jonayat ASM, Janik MJ, Senftle TP. Interaction trends between single metal atoms and oxide supports identified with density functional theory and statistical learning. *Nat Catal* **1**, 531-539 (2018).
55. Andersen M, Levchenko SV, Scheffler M, Reuter K. Beyond Scaling Relations for the Description of Catalytic Materials. *ACS Catal* **9**, 2752-2759 (2019).
56. Zunger A. Systematization of the stable crystal structure of all AB-type binary compounds: A pseudopotential orbital-radii approach. *Phys Rev B* **22**, 5839-5872 (1980).
57. Ouyang R, Curtarolo S, Ahmetcik E, Scheffler M, Ghiringhelli LM. SISSO: A compressed-sensing method for identifying the best low-dimensional descriptor in an immensity of offered candidates. *Physical Review Materials* **2**, 083802 (2018).
58. Calle-Vallejo F*, et al.* Finding optimal surface sites on heterogeneous catalysts by counting nearest neighbors. *Science* **350**, 185-189 (2015).
59. Wang L*, et al.* Tunable intrinsic strain in two-dimensional transition metal electrocatalysts. *Science* **363**, 870-874 (2019).
60. Yan Y, Du JS, Gilroy KD, Yang D, Xia Y, Zhang H. Intermetallic Nanocrystals: Syntheses and Catalytic Applications. *Adv Mater* **29**, 1605997 (2017).
61. Gilroy KD, Ruditskiy A, Peng H-C, Qin D, Xia Y. Bimetallic Nanocrystals: Syntheses, Properties, and Applications. *Chem Rev* **116**, 10414-10472 (2016).
62. Cui Z*, et al.* Synthesis of Structurally Ordered Pt3Ti and Pt3V Nanoparticles as Methanol Oxidation Catalysts. *J Am Chem Soc* **136**, 10206-10209 (2014).
63. Luo M*, et al.* PdMo bimetallene for oxygen reduction catalysis. *Nature* **574**, 81-85 (2019).
64. Wang Z-T*, et al.* Preparation, Structure, and Surface Chemistry of Ni–Au Single Atom Alloys. *J Phys Chem C* **120**, 13574-13580 (2016).
65. Lacey SD*, et al.* Stable Multimetallic Nanoparticles for Oxygen Electrocatalysis. *Nano Lett* **19**, 5149-5158 (2019).
66. Yao Y*, et al.* Carbothermal shock synthesis of high-entropy-alloy nanoparticles. *Science* **359**, 1489-1494 (2018).
67. Tao F*, et al.* Break-Up of Stepped Platinum Catalyst Surfaces by High CO Coverage. *Science* **327**, 850-853 (2010).
68. van Spronsen MA*, et al.* Dynamics of Surface Alloys: Rearrangement of Pd/Ag(111) Induced by CO and O2. *J Phys Chem C* **123**, 8312-8323 (2019).